Synthesis and characterization of magnetic iron sulfide (Fe-S)/CuS nanocomposite as a novel recyclable catalyst in photocatalyst removal of tetracycline from aqueous solutions

Haniyeh Rasouli Darmiyan[a], Rasoul Khosravi[b], Taher Shahryari[b],*

[a]Student Research Committee, Faculty of Health, Birjand University of Medical Sciences, Birjand, Iran,
email: haniyeh_rasouli@yahoo.com
[b]Social Determinants of Health Research Center, Department of Environmental Health Engineering, Faculty of Health, Birjand University of Medical Sciences, Birjand, Iran, emails: shahryaritaher@yahoo.com (T. Shahryari), khosravi.r89@gmail.com (R. Khosravi)

ABSTRACT

Drugs, especially antibiotics, as a group of emerging contaminants, pose a serious threat to the environment and aquatic ecosystems due to their adverse effects, cumulative properties, and developing drug resistancy. Therefore, this study aimed to evaluate the removal efficiency of tetracycline (TC) antibiotic from aqueous solutions using photocatalytic process in the presence of magnetic iron sulfide (Fe-S/CuS) nanoparticles on a laboratory scale. The magnetic nanocomposite was first characterized by transmission electron microscopy, X-ray diffractometer, vibration sampling magnetometer, Field-emission scanning electron microscopy, Fourier-transform infrared spectrometer, diffuse reflection spectroscopy, and energy-dispersive X-ray spectroscopy techniques. Factors, such as pH, reaction contact time, nanocomposite dose, and contaminant concentration on the removal efficiency were studied. All the experiments were performed at room temperature under UV-A light. The results of this study indicated that the highest removal efficiency of TC was obtained at optimum pH of 7. The results also showed that in the initial concentration of TC antibiotic (20 mg/L), the removal efficiency increased by increasing contact time and also by increasing the dose of the desired nanocomposite, the removal efficiency first increased and then decreased. Moreover, the synthesized nanocomposite had the ability to be reused with an 18% reduction in the removal efficiency in five consecutive cycles. Finally, the results of this study showed the acceptable efficiency of Fe-S/CuS nanocomposite in photocatalytic removal of TC antibiotic.

Keywords: Photocatalytic process; Tetracycline; Magnetic nanocomposite; UV-A light

1. Introduction

In aquatic ecosystems, persistent organic pollutants are important environmental issues due to their high toxicity, solubility, and carcinogenicity [1]. Among the organic substances, drugs cause great concern due to continuous detection in aquatic environments, although they are considered as a turning point in human scientific progress. Incomplete removal of them during the wastewater treatment process indicates that treatment plants are not designed to remove medicinal products. Therefore, pharmaceutical effluents are described as an important source of concern for emerging pollutants [2,3].

Antibiotics have been used as therapeutic agents in the treatment of infectious diseases of humans and animals and today are used as food additives as preventers and growth stimulants in the livestock and aquaculture industries. These pollutants can enter the aquatic environment

* Corresponding author.

through the effluent and sludge of hospitals, health centers, domestic wastewater treatment plants, pharmaceutical and agricultural industries, and livestock farms. They have raised many concerns about health risks to humans and animals due to their persistence and accumulation in the environment [4].

The tetracycline (TC) antibiotic with the chemical formula $C_{22}H_{24}N_2O_8$ and a molecular weight of 444.435 g/mol [5] is a known emerging contaminant. However, due to some positive aspects, such as low cost, wide spectrum, and high antimicrobial activity [6], it is the second most widely used drug in the world in aquaculture, animal husbandry, and treatment of humans and animals [7]. Due to incomplete absorption and metabolism, large amounts of this contaminant are continuously discharged through the feces or urine of animals and humans into domestic sewage and agricultural runoff, which cannot be completely removed by traditional wastewater treatment processes [8].

Even low allowed concentrations of TC in the environment can pose many risks to ecosystems and human health due to bacterial resistance to antibiotics and low degradability of its molecules.

Therefore, it is critical to remove these molecules before being discharged into water sources [10]. Several methods can be used to remove TC from aqueous environments, including ultraviolet [11], Fe nanoparticles [12], adsorption [13] coagulation, Fenton-like processes and other advanced oxidation processes (AOPs) [14,15], photocatalyst [16], nanofiltration [17], carbon nanotubes [18], and etc. Despite their advantages, these processes also have disadvantages making them difficult to use.

Photocatalytic degradation of organic compounds is a common method in water and wastewater treatment [19]. In the treatment of persistent wastewater, the photocatalytic oxidation process has been widely used due to its advantages, such as no secondary pollution and energy saving [20]. In this method, pollutants are not transferred from one phase to another; they are converted into safe compounds, such as CO_2, H_2O, and etc. [21].

Due to the unstable nature of effluents containing organic pollutants, AOPs are widely used for treatment of this type of wastewater, especially antibiotics. In addition, it is an effective approach with high efficiency and Full mineralization [22,23].

In photocatalytic process, as an AOP, organic matter is decomposed in the presence of metal dioxide and under ultraviolet radiation. In other words, in this mechanism, by irradiating ultraviolet radiation to the semiconductor material and exciting electrons from the valence band to the conduction band, hydroxyl radicals are produced in aqueous solutions [24]. The process of photolysis is the interaction of natural or artificial light with target molecules and the induction of chemical reactions causing direct degradation of contaminants to intermediate products [25].

Iron sulfide (FeS), a tetragonal ferrous monosulfide, is the first solid phase of crystalline FeS formed under sulfate reduction conditions. FeS is a non-toxic and ubiquitous mineral that can be easily synthesized. FeS is used in the treatment of groundwater and soils contaminated with heavy metals, organic chlorine compounds, arsenic, selenium, and other inorganic and organic pollutants [26].

Synthetic and nano (micro) FeS scale shows much higher capacity and efficiency in immobilization and removal of metals due to greater specific area and higher reactivity. This low-cost, high-surface area material with good properties is synthesized by a simple and inexpensive method using a new laboratory method without the need for stabilization. The nanocomposite is eco-friendly, so that it can eventually be used as agricultural fertilizer [27,28].

Another important semiconductor material with physical, chemical, electrical, and magnetic properties is copper sulfide (CuS) with a bandwidth of 0.2 electron volts [29]. Ability to absorb a wide range of electromagnetic waves and high efficiency in photocatalytic degradation of organic compounds are important advantages of such materials. Moreover, high chemical stability, non-toxicity, no mass transfer limitation, high resistance to chemical decomposition, and optical corrosion are other important advantages of this catalytic process. Today, semiconductors, such as CuS, are used to remove pollutants from aqueous media using various processes [30]. Therefore, this study aimed to evaluate the photocatalytic degradation of TC antibiotic from aqueous solutions in the presence of UV-A light by Fe-S/CuS nanocomposite.

2. Materials and methods

2.1. Materials

For Fe-S synthesis, iron(II) sulfate [$FeSO_4·7H_2O$], sodium thiosulfate [$Na_2S_2O_3$], sodium hydroxide [NaOH], and sulfuric acid [H_2SO_4] were used, all of which are listed as industrial, commercial, and inexpensive raw materials.

For Fe-S/CuS nanocomposite synthesis, copper sulfate [$CuSO_4$], ethylene glycol [$C_2H_6O_2$] (99%), sodium thiosulfate [$Na_2S_2O_3$], and 99.6% ethyl alcohol were used. In addition, TC powder [$C_{22}H_{24}O_8N_2·HCl$] (Sigma-Aldrich) was used to prepare different concentrations of the contaminant solutions and deionized water was used to prepare the solutions in all stages.

2.2. Synthesis of Fe-S nanocomposite

At this stage, a few drops of concentrated sulfuric acid were added to a beaker containing 0.8 L of distilled water. After placing on the heater and reaching the desired solution temperature of 85°C–80°C and setting up a water bath, 1 g of iron(II) sulfate [$FeSO_4·7H_2O$] was added to the solution and stirred until completely dissolved. Then 2.5 g sodium thiosulfate [$Na_2S_2O_3$] and about 0.9 g sodium hydroxide (NaOH) were added step by step at the desired temperature. It was continuously stirred until an alkaline, black solution (pH > 14), representing the nanocomposite synthesis, was formed. Finally, after cooling, the solution was washed with distilled water until it reached a neutral pH and dried.

2.3. Synthesis of Fe-S/CuS nanocomposite

At this stage, 0.15 g of the previously prepared Fe-S nanocomposite was dispersed in 20 mL of ethylene glycol for 30 min in ultrasonic equipment. The obtained solution was then poured into a 500 cc volumetric flask and placed in an oil bath at 120°C. After that, 0.8 g of copper sulfate was added

and completely dissolved in the volumetric flask. After this step, 1.9 g of sodium thiosulfate [$Na_2S_2O_3$], which was added separately in 20 mL of ethylene glycol (EG), was poured into the solution in the volumetric flask and the sample was refluxed at 140°C for 90 min. After cooling the solution, the synthesized material was separated by N_{42} magnet and washed first with ethanol and then several times with deionized water and finally was dried at 80°C in an oven for 5 h.

2.4. Characterization of the synthesized nanocomposite

XRD analysis (X-ray diffractometer) was done using Bruker AXS-D8 Advance, Germany, to investigate the composition and characterization of the crystal structure of the synthesized Fe-S/CuS nanocomposite. FE-SEM analysis (Field-emission scanning electron microscopy) was done using TESCAN Vega3 to study the morphology, shape, average diameter, and estimate the size of the synthesized Fe-S/CuS nanocomposite in micro and nano dimensions. In order to determine the type and percentage of constituent elements on the synthesized catalyst, EDX (energy-dispersive X-ray spectroscopy) was performed using TESCAN Vega3. A VSM (vibration sampling magnetometer) model 7407, Lake Shore Cryotronics Co., United States, was used to determine magnetic properties of the synthesized magnetic nanoparticles. FTIR analysis (Fourier-transform infrared spectrometer) was performed by PerkinElmer-Spectrum 65 with a wavelength of 1–400 cm to 1–4,000 cm to identify the functional groups in the molecular structure of the produced nanoparticles. In order to measure the interaction of light and the synthesized material, DRS (diffuse reflection spectroscopy) was performed by a device model UV-2550, Shimadzu Co., Japan. Finally, TEM analysis (transmission electron microscopy) as a microscopy technique was performed by a device model EM208S, Philips Co., Netherlands.

2.5. Photocatalytic removal experiments

First, 100 mg/L stock solution was weekly prepared by dissolving TC powder in deionized water. This solution was stored in the refrigerator at 4°C. The studied variables included pH (3, 5, 7, 9, and 11), contaminant concentration (5, 10, 20, 50, and 100 mg/L), nanocatalyst dose (0.05, 0.1, 0.25, 0.5, 0.75, and 1 g/L), and contact time (5, 10, 15, 30, 45, 60, 90, 120, and 180 min). The solution pH was adjusted by a pH meter (Knick–Calimatic), Germany, using choloridric acid and 0.1 N NaOH. All the experiments were performed at room temperature in a batch reactor using 100 mL samples on a magnetic stirrer with a mixing speed of 150 rpm in the presence of UV-A light.

The samples were prepared according to the specified parameters, and after separating the nanocomposite by a magnet, the residual concentration of the contaminant was measured by DR6000 UV/Vis spectrophotometer with a wavelength of 358 nm according to the Standard Methods for the Examination of Water and Wastewater [31].

The removal efficiency of TC contaminant was calculated according to Eq. (1).

$$R(\%) = \frac{(C_0 - C_t)}{C_0} \times 100 \tag{1}$$

where C_t and C_0 indicate TC concentration at time t and the initial concentration of TC (mg/L); R% indicates the contaminant removal efficiency.

To determine the possible amount of iron leaked into the solution, the amount of it was measured according to methods 3500A and 3111B and C of the Standard Methods for Water and Wastewater Testing and by the atomic absorption spectrometric device made by VARIAN Company in Australia.

2.6. Recovery and composite reuse tests

Evaluation of stability and reuse of solid catalysts is one of the important parameters. In the present study, to investigate the synthesized nanocomposite in the presence of UV-A light in order to degrade the TC contaminant, the experiments were performed in five alternating cycles and photocatalytic experiments under optimal conditions. The desired magnetic nanocatalyst (Fe-S/CuS nanocomposite) was separated from the solution by N_{42} magnet in each cycle and washed with deionized water in several stages and dried in a vacuum oven at 80°C. Then the next removal cycle was performed with the same dose of nanocomposite. Residual contaminant concentrations were separately measured after each cycle of the photocatalytic degradation process.

3. Results and discussion

3.1. Characteristics of the synthesized nanocomposite

3.1.1. XRD analysis

The crystallinity of powder and solid materials was detected by XRD analysis. Fig. 1 shows the XRD pattern of Fe-S and Fig. 1 reveals the XRD pattern of the Fe-S/CuS nanocomposite. Accordingly, at 2θ equal to 30.79°, 35.44°, 53.84°, 57.54°, 63.04°, and 74.54°, peaks related to the presence of iron in the nanocomposite can be seen in the figure.

Moreover, the peaks related to CuS equal to 29.34°, 31.84°, 32.14°, 48.04°, 53.09°, and 59.89°, can be seen in Fig. 1 [32].

3.1.2. FE-SEM analysis

This analysis was used to investigate the surface properties of different samples. Fig. 2 reveals that most of the particles are in the nanoscale range; some aggregated particles are also present. In Fig. 2a, a micrograph with a magnification of 40.0 KX taken from Fe-S nanocomposite of FeS particles is well and uniformly observed, which is indicated by the dark spots in the image. Fig. 2b shows the Fe-S/CuS nanocomposite with a magnification of 25.0 KX after loading CuS on the previous nanocomposite. As shown in the figure, CuS is placed on the substrate and given that the nanocomposite has magnetic properties, there is a possibility of accumulation in them [33,34].

3.1.3. DRS analysis

DRS was performed to evaluate the optical properties of the composite used in this study. According to previous studies related to FeS and CuS nanocomposites, band gap
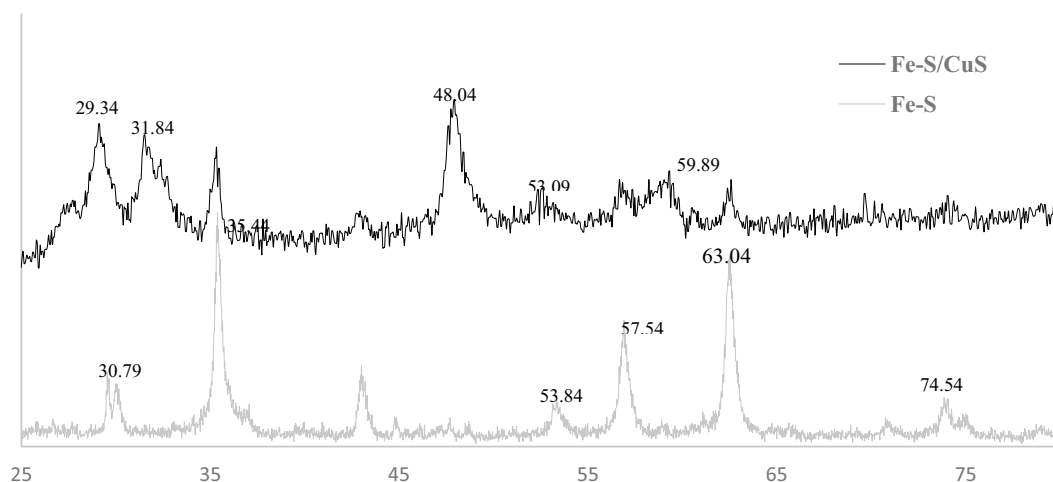
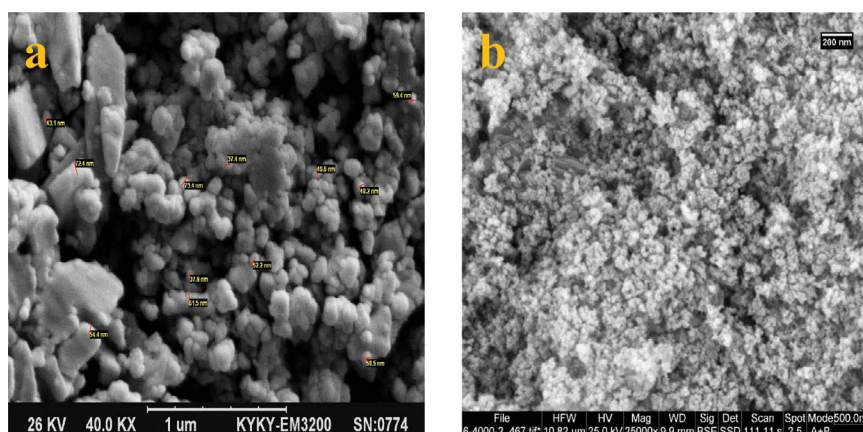Fig. 1. XRD patterns of Fe-S and Fe-S/CuS.

Fig. 2. FE-SEM images related to the (a) Fe-S and (b) Fe-S/CuS nanoparticles.

alone is about 2; however, the study of this analysis showed that the presence of other materials in the synthesized magnetic nanocomposite (Fe-S/CuS) caused a slight change in the CuS band gap. According to Fig. 3, the nanocomposite has a stronger and better absorption in the light range of 300–700 nm, indicating the suitability of the synthesized composite in photocatalytic processes in the range of visible light and sunlight [33].

The band gap energy of Fe-S/CuS based on the formula $E_g = 1239.8/\lambda$ is equal to 1.68 electron volts. On the other hand, the band gap energy of Fe-S/CuS after the process was 5.34 electron volts. This indicates that the metal portion of the synthesized nanocomposite, that is, FeS and CuS elements, might decreased, which EDX analysis diagrams explain the difference in band gap before and after the photocatalytic process [35].

3.1.4. FTIR analysis

In order to further study the quality of Fe-S/CuS samples, FTIR analysis was performed in the range of 500–4,000 cm⁻¹. Fig. 4 reveals that in the corresponding spectrum at 563.25 cm⁻¹, the C–O functional group is clearly identified.

Moreover, peaks of 500 to 1,000 cm⁻¹ can be attributed to the functional groups Fe–O–OH and Fe–O. Peaks of 777.48, 891.99, and 911.66 cm⁻¹ are probably related to Fe-S stretching. Two peaks of 1,061.49 and 1,212.35 are observed in the spectrum, which are related to the bond of stretching vibrations S=S and asymmetric stretching vibrations C=C, respectively [36,37].

3.1.5. EDX analysis

EDX analysis was conducted for studying structural or chemical properties of a sample. According to Fig. 5 related to the synthesized nanocomposite, the presence of Cu, S, and Fe elements is observed close to the stoichiometric ratio. The figure also shows the presence of elements related to the semiconductor composition of CuS as the last layer of the composite [38].

3.1.6. VSM analysis

Due to the fact that the nanocatalyst used in this study has magnetic properties, VSM was used to investigate the magnetic properties. Fig. 6 show that the saturation
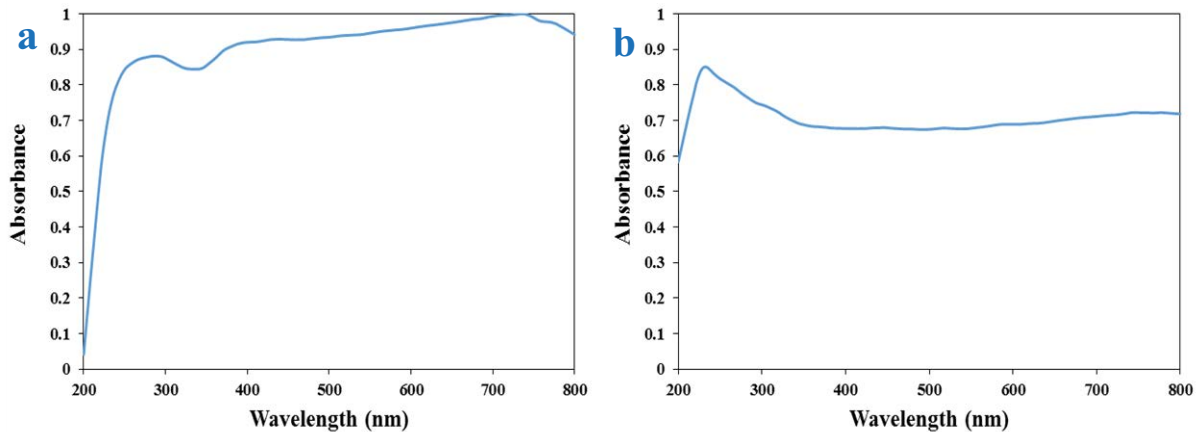
Fig. 3. DRS analysis of Fe-S/CuS nanoparticles (a) before TC and (b) after TC degradation.
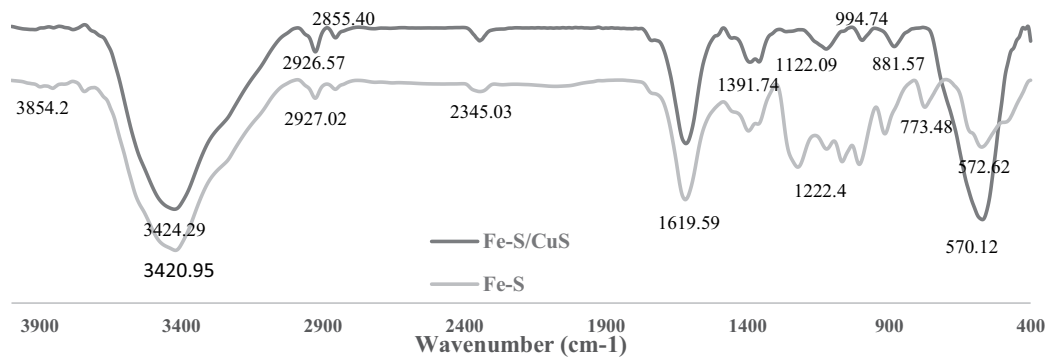

Fig. 4. FTIR spectra of Fe-S and Fe-S/CuS.

magnetization of this nanoparticle before modification is about 90 emu/g and its coercivity is about 76 G. However, characteristic values of modified Fe-S/CuS nanocomposite in the study are 11 emu/g and 91 G, respectively. According to the mentioned properties and the mentioned curves, it can be concluded that this ferromagnetic material has very good soft magnetic properties. This property facilitates the separation of this nanocomposite and makes it easy to be separated by a magnet [28].

3.1.7. TEM analysis

The particle size of Fe-S/CuS nanocomposite was determined by TEM analysis. Fig. 7 reveals that the Fe-S/CuS particle size is in the nanoscale range and is relatively spherical. The almost irregular cumulative state of the particles is also due to the high magnetic properties of this nanocomposite [39].

3.2. Parameters affecting the photocatalytic degradation of TC antibiotic

3.2.1. pH effect

Many studies have emphasized the role of pH as one of the most important and influential parameters in AOPs

in removing antibiotics. It is due to the fact that pH has a great effect on the rate of pollutant decomposition, adsorption capacity, charge distribution on the photocatalyst surface, and the oxidation potential of valence band [40,41]. The TC antibiotic, as an amphoteric molecule, consists of three functional groups, including tricarbonyle methane group, phenolic deketone group, and dimethyl amino group. These functional groups at different pH and in aqueous media have different acid dissociation constant (pKa) [42,43].

It is worth mentioning that the concentration of H^+ protons increases by decreasing pH (tendency to acidic media), thus leading to competition between protons and TC molecules for negatively charged sites of the catalyst. Therefore, at acidic pH, an increase in H^+ concentration leads to the formation of $-OH_2^+$ species, making the surface of the catalyst positive and leads to repulsion of TC molecules by electrostatic forces [44].

Many studies have indicated that the highest and best oxidation capacity in photocatalytic processes for TC contaminants occur in the range of neutral and especially alkaline pH. The present study also confirms this result; since the results of the study in Fig. 8 show that after 30 min at pH = 3, the pollutant removal was 42.19% and by increasing pH the removal efficiency increased, so that at the same time (after 30 min) TC removal efficiency was 83.54% and 86.07% at pH 7 and pH 9, respectively. The results of the study by
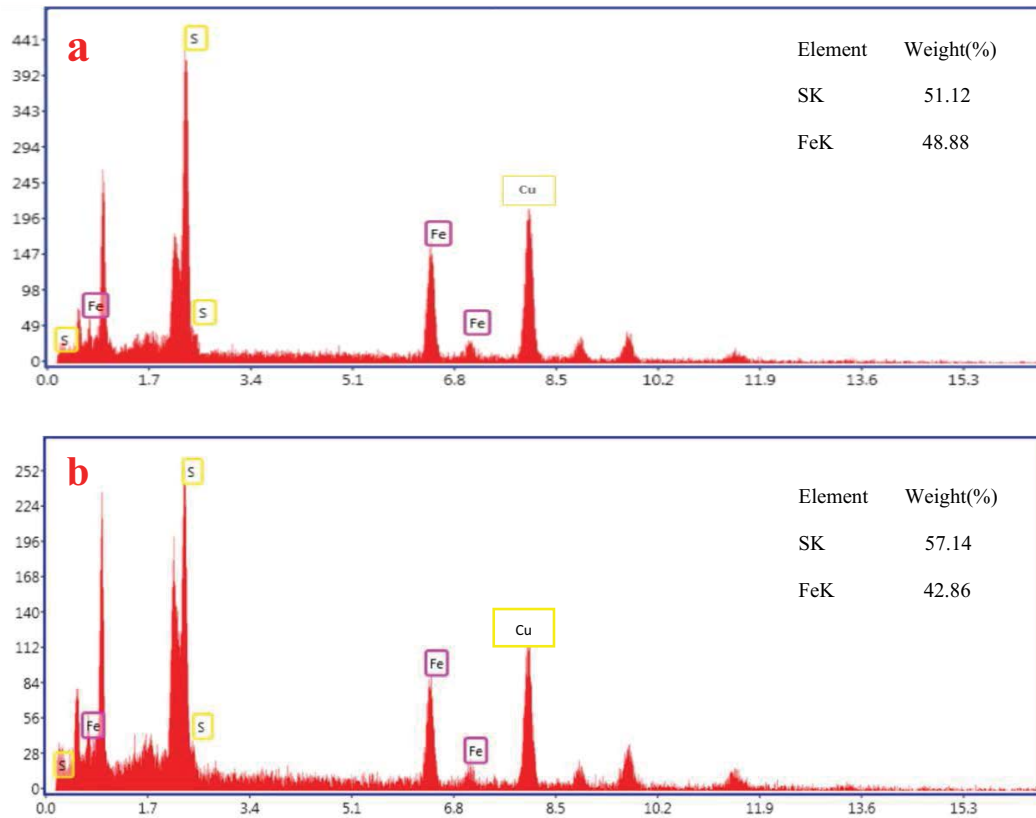
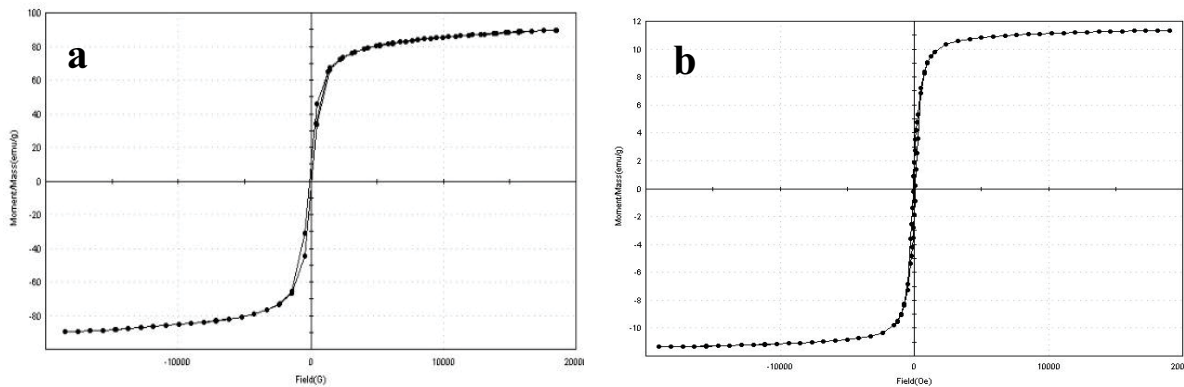Fig. 5. EDX analysis of Fe-S/CuS nanoparticles (a) before TC and (b) after TC degradation.

Fig. 6. VSM analysis of (a) Fe-S and (b) Fe-S/CuS nanoparticles.

Xue et al. [45], Ma et al. [46], and Wang et al. [47] are also in line with the results of the present study. For further comparison and review, at the same parameters the adsorption efficiency was 45.56% and 43.03% at pH = 7 and pH = 9.

The semiconductor photocatalytic mechanism can be divided into steps, such as transfer of reactants in the liquid phase to the catalyst surface, their adsorption on the catalyst, reaction in the adsorbed phase on the catalyst, desorption of products from the catalyst surface, and dispersion of decomposition products. Photocatalysts are materials producing hydroxyl radicals in aqueous solutions that have oxidizing properties by irradiating ultraviolet light to a semiconductor material and exciting electrons from the capacitance band to the conduction band. The photocatalytic process in this study begins in the presence of a Fe-S/CuS catalyst by absorbing a photon with energy equal to or greater than the band gap energy of the catalyst particles, which produces an electron–hole pair. In the presence of particles adsorbed on the surface of the catalyst, such as water, OH^-, and oxygen, hydroxyl radicals are formed due to the high oxidation potential of the holes. As a result, the TC contaminant is degraded
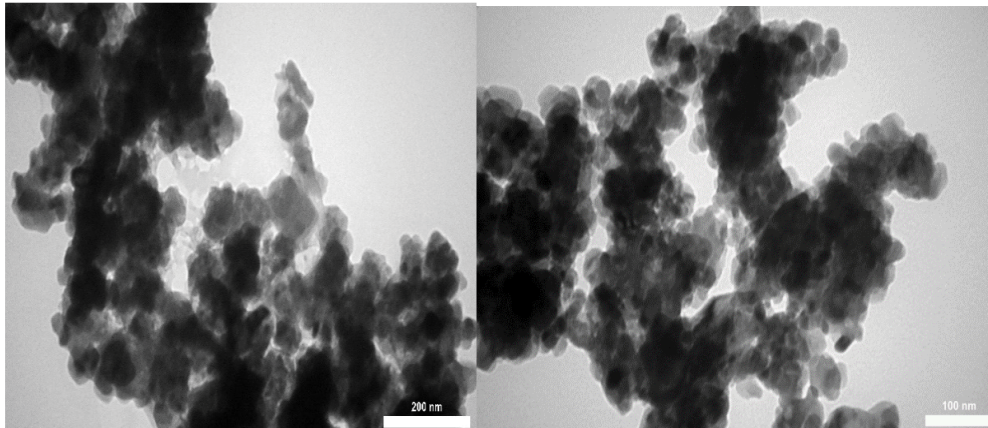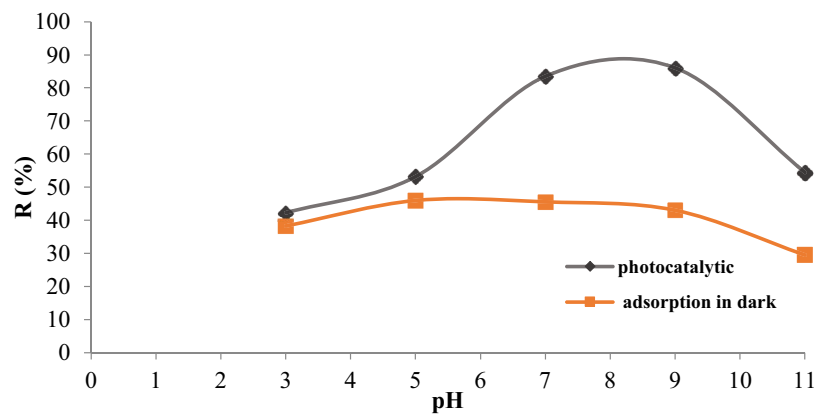
Fig. 7. TEM images of Fe-S/CuS.

Fig. 8. Effect of pH changes on the TC degradation in photocatalytic processes (TC concentration = 20 mg/L, nanocomposite dose = 0.5 g/L, time: 30 min, and ambient temperature).

by indirect oxidation through hydroxyl radicals or by direct oxidation through the valence-band hole [48–51].

The mechanism of the photocatalytic process of TC removal along with the reactions performed in this process is shown in Fig. 9.

The samples after the photocatalytic process were evaluated by a high-performance liquid chromatograph (HPLC, LC-10AT, Shimadzu, Japan) fixed up with a C-18 column, to find the possible intermediate by-products. The main degradation by-products of TC were phthalic acid mono-2-ethylhexyl ester ($C_{16}H_{22}O_4$), 3,8-dimethyldecane ($C_{12}H_{26}$) and decane, 4-ethyl ($C_{12}H_{26}$). During the first stages, the reactivity of hydroxyl radicals, multiple hydroxylation reactions happened. Then compounds with lower molecular weight produced by leakage of aromatic rings. Ultimate ring-opening leads to the formation of short-chain carboxylic acids, which are eventually mineralize to CO_2, water and inorganic ions [52–55].

3.2.2. Effect of magnetic nanocomposite dose

Another important parameter is the effect of the synthesized catalyst dose, which is very important in photocatalytic processes. In order to investigate the effect of nanocomposite dose on photocatalytic removal of TC,

different amounts (0.05, 0.1, 0.25, 0, 5, 0.75, and 1 g/L) of Fe-S nanocomposite were tested in the presence of UV-A light. To investigate this variable, the experiments were performed on the desired contaminant solution with a concentration of 20 mg/L at optimum pH of 7. Fig. 10 shows that the removal efficiency of TC contaminant first increases and then decreases by increasing the catalyst dose in the presence of UV-A light. So that after 30 min at doses of 0.25, 0.5, and 0.75 g/L, the pollutant removal was 56.11%, 83.11%, and 90.08%, respectively, but at a dose of 1 g/L, the removal efficiency decreased to 85.23%. Therefore, increasing the nanocomposite dose in the solution, turbidity is created, disrupting the light distribution in the solution, and as a result, the removal efficiency of TC decreases. This result is consistent with the study by Xue et al. [45].

3.2.3. Effect of TC concentration

In this part of the study, to determine the effect of TC initial concentration on photocatalytic removal efficiency, different concentrations of TC (5, 10, 20, 50, and 100 mg/L) were exposed to UV-A light for 30 min, with the optimal dose of nanocomposite (0.5 g/L), and optimum pH of 7. Fig. 11 shows that by increasing concentration, the removal efficiency of TC antibiotic significantly reduces.
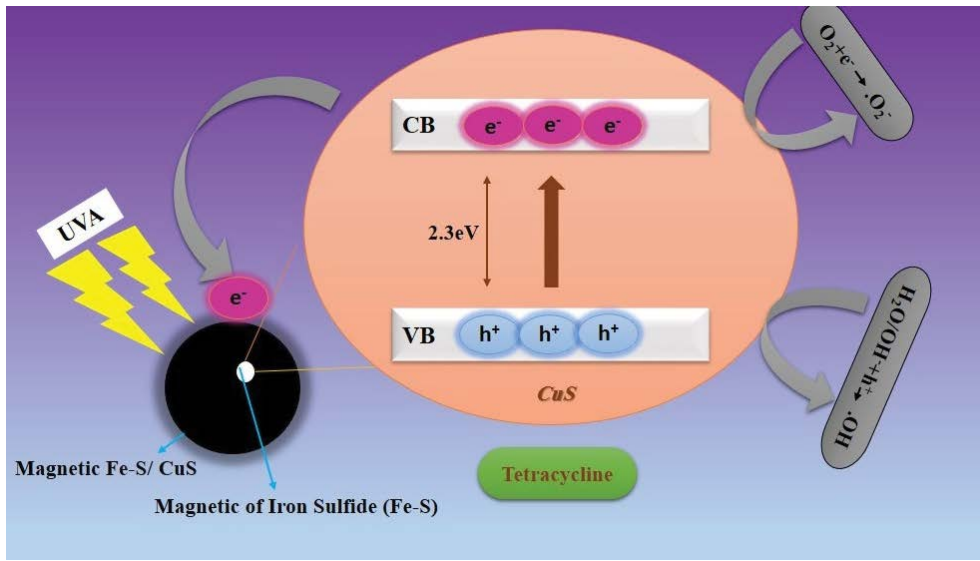
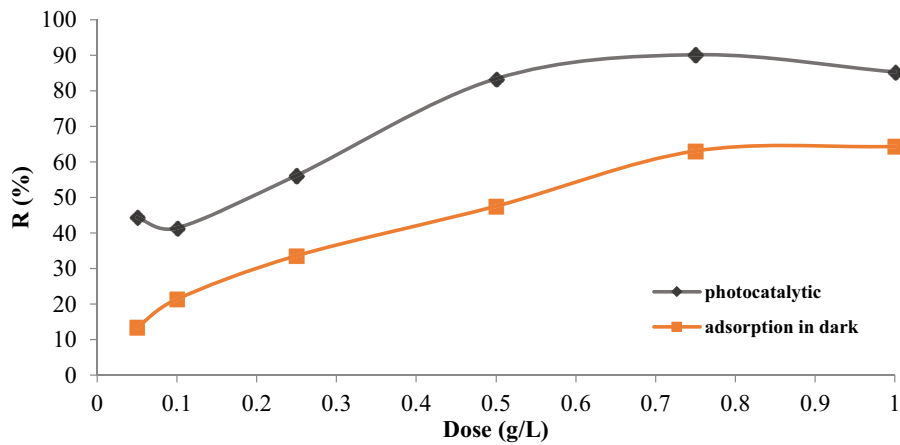Fig. 9. Mechanism of the photocatalytic process of TC.

Fig. 10. Effect of nanocomposite dosage on the TC degradation in photocatalytic processes (TC concentration = 20 mg/L, pH = 7, time: 30 min, and ambient temperature).
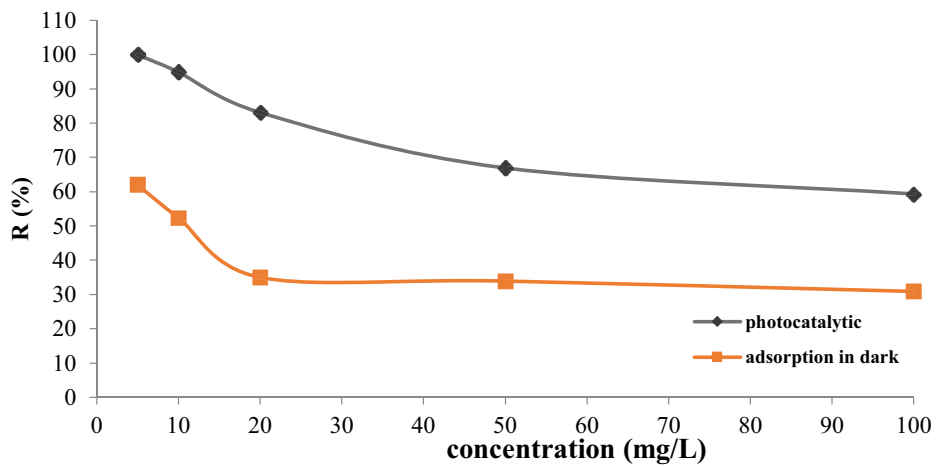

Fig. 11. Effect of changes in the initial TC concentration on its degradation efficiency in photocatalytic processes (pH = 7, nanocomposite dose = 0.5 g/L, time: 30 min, and ambient temperature).

The removal efficiency of TC contaminant in 30 min at a concentration of 10 mg/L was 94.93%, but this efficiency at the initial concentrations of 20, 50, and 100 mg/L was 83.12, 66.91, and 59.32, respectively. The adsorption efficiency was 35.02% at the initial concentrations of 20 mg/L. The removal efficiency decreased by increasing concentration; since at lower concentrations, the reaction of the desired contaminant with OH radicals increases and ultimately leads to increased degradation of this contaminant by free radicals. Furthermore, by increasing the contaminant concentration, light does not reach the surface of all catalyst particles and catalyst sections are not affected by UV-A light. In the study by Nasseh et al. [29], photocatalytic removal of TC was performed, the results of which were consistent with the results obtained in the present study [42].

3.2.4. Effect of TC contact time

In this part, to determine the effect of contact time on the photocatalytic removal efficiency of TC, different contact times (5, 10, 15, 30, 45, 60, 90, 120, and 180 min) on 20 mg/L of the contaminant solution, with optimal dose of nanocomposite (0.5 g/L) and optimum pH of 7 were exposed to UV-A light. Fig. 12 reveals that by increasing contact time, the removal efficiency of the TC antibiotic increased;

at contact time of 180 min, the removal efficiency reached 100%. At time of 30 and 45 min the pollutant removal efficiency also reached 82.27%, 84.17%, and 89.45%, respectively. The results of the study by Nasseh et al. [29] on this pollutant, were consistent with the results the current study. It is noteworthy that UV-A light radiation alone does not have a significant efficiency in removing TC. The results showed that removal efficiency of light alone (photooxidation) in 180 min was 56.72%; however, it reached 100% in similar conditions and in the presence of an optimal dose of nanocomposite [56,57]. In addition, the adsorption efficiency was 35.75% at the same parameters.

3.3. Investigating Fe-S/CuS magnetic nanocomposite reuse in the process of TC photocatalytic degradation

This study investigated the magnetic recovery capability of Fe-S/CuS nanocomposite in TC photocatalytic degradation. To this end, after each use of nanocomposite and degradation of the pollutant under UV-A light for photocatalytic process in 30 min and optimal process conditions, the nanocomposite was separated from the solution by a magnet. Then, it was washed with distilled water and ethanol at 80°C and dried in a vacuum oven for 8 h, and it was reused in the pollutant degradation process. Fig. 13 shows
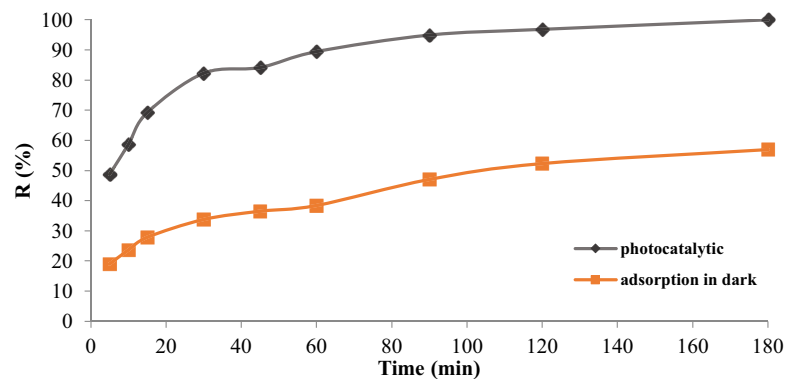

Fig. 12. Effect of time changes on the TC degradation in photocatalytic processes (TC concentration = 20 mg/L, nanocomposite dose = 0.5 g/L, pH = 7, and ambient temperature).
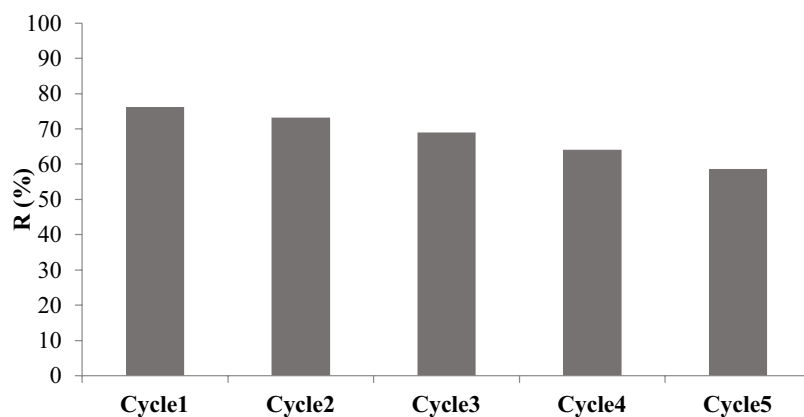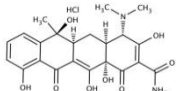

Fig. 13. Diagram of TC degradation in during 5 cycles of reuse in the presence of Fe-S/CuS nanocomposite (TC concentration = 20 mg/L, nanocomposite dose = 0.5 g/L, pH = 7, and time: 30 min).

Table 1
Chemical characteristics of TC [9]

TC	Chemical formula	Molecular weight (g/mol)	Solubility (mol/L)	pKa$_1$	pKa$_2$	pKa$_3$	Chemical structure
TC	$C_{22}H_{24}N_2O_8 \cdot HCL$	444.435	0.041	3.3	7.8	9.7	

the results of magnetic recovery of the nanocomposite. The photocatalytic efficiency of the sample reduced by about 18%, after 5 times of using the nanocomposite. This can be due to the reduction of the catalyst (separation process and reduction of the optimal nanoparticle dose) as well as the change in the structure of the catalyst due to light reactions [58]. The degradation rate of TC after 5 times of using the nanocomposite, was about 58.64%. The synthesized nanocomposite was easily separated from the solution after being placed on the magnet and centrifuged for 5 min; this feature is very suitable for the recovery of the nanocomposite.

4. Conclusion

This study aimed to synthesize Fe-S/CuS magnetic nanocomposite in the removal of TC antibiotic from aqueous media under the influence of UV-A light and to investigate various variables, including pH, initial contaminant concentration, and nanocomposite dose at different times. The results indicated that the nanocatalyst has good efficiency in TC photocatalytic degradation. Moreover, under optimal conditions (pH = 7, catalyst dose of 0.5 g/L, contaminant concentration of 20 mg/L, contact time of 30 min, and room temperature) the efficiency of photocatalytic degradation process was 82.27%. By increasing the nanocatalyst dose, the removal efficiency first increased and then decreased, which is due to interference in the penetration of UV-A light emitted into the sample. Given the good efficiency of the synthesized nanocomposite (Fe-S/CuS) in TC photocatalytic degradation process as well as its relatively simple and economical synthesis and easy separation with N_{42} magnet, it can be used as a suitable catalyst in removing and degrading persistent organic pollutants. The amount of examined metal was zero.

Acknowledgment

References

[1] H. Wang, Y. Wu, M.B. Feng, W.G. Tu, T. Xiao, T. Xiong, H.X. Ang, X.Z. Yuan, J.W. Chew, Visible-light-driven removal of tetracycline antibiotics and reclamation of hydrogen energy from natural water matrices and wastewater by polymeric carbon nitride foam, Water Res., 144 (2018) 215–225.

[2] N. Malesic-Eleftheriadou, E.N. Evgenidou, G.Z. Kyzas, D.N. Bikiaris, D.A. Lambropoulou, Removal of antibiotics in aqueous media by using new synthesized bio-based poly(ethylene terephthalate)-TiO$_2$ photocatalysts, Chemosphere, 234 (2019) 749–755.

[3] N. Nasseh, B. Barikbin, L. Taghavi, M.A. Nasseri, Adsorption of metronidazole antibiotic using a new magnetic nanocomposite from simulated wastewater (isotherm, kinetic and thermodynamic studies), Composites, Part B, 159 (2019) 146–156.

[4] S.J. Segovia-Sandoval, L.M. Pastrana-Martínez, R. Ocampo-Pérez, S. Morales-Torres, M.S. Berber-Mendoza, F. Carrasco-Marín, Synthesis and characterization of carbon xerogel/graphene hybrids as adsorbents for metronidazole pharmaceutical removal: effect of operating parameters, Sep. Purif. Technol., 237 (2020) 116341, doi: 10.1016/j.seppur.2019.116341.

[5] J.J. Yu, J. Kiwi, I. Zivkovic, H.M. Rønnow, T.H. Wang, S. Rtimi, Quantification of the local magnetized nanotube domains accelerating the photocatalytic removal of the emerging pollutant tetracycline, Appl. Catal., B, 248 (2019) 450–458.

[6] T. Ahamad, Mu. Naushad, T. Al-Shahrani, N. Al-Hokbany, S.M. Alshehri, Preparation of chitosan based magnetic nanocomposite for tetracycline adsorption: kinetic and thermodynamic studies, Int. J. Biol. Macromol., 147 (2020) 258–267.

[7] C.K. Wang, C.-Y. Lin, G.-Y. Liao, Degradation of antibiotic tetracycline by ultrafine-bubble ozonation process, J. Water Process Eng., 37 (2020) 101463, doi: 10.1016/j.jwpe.2020.101463.

[8] N.A. Al-Dhabi, G.A. Esmail, M.V. Arasu, Effective degradation of tetracycline by manganese peroxidase producing *Bacillus velezensis* strain Al-Dhabi 140 from Saudi Arabia using fibrous-bed reactor, Chemosphere, 268 (2021) 128726, doi: 10.1016/j.chemosphere.2020.128726.

[9] M. Khodadadi, M.H. Ehrampoush, M.T. Ghaneian, A. Allahresani, A.H. Mahvi, Synthesis and characterizations of FeNi$_3$@SiO$_2$@TiO$_2$ nanocomposite and its application in photocatalytic degradation of tetracycline in simulated wastewater, J. Mol. Liq., 255 (2018) 224–232.

[10] S.-M. Alatalo, E. Daneshvar, N. Kinnunen, A. Meščeriakovas, S.K. Thangaraj, J. Jänis, D.C.W. Tsang, A. Bhatnagar, A. Lähde, Mechanistic insight into efficient removal of tetracycline from water by Fe/graphene, Chem. Eng. J., 373 (2019) 821–830.

[11] A. Tiwari, A. Shukla, Lalliansanga, D. Tiwari, S.-M. Lee, Au-nanoparticle/nanopillars TiO$_2$ meso-porous thin films in the degradation of tetracycline using UV-A light, J. Ind. Eng. Chem., 69 (2019) 141–152.

[12] Y. Wu, Q. Yue, Y. Gao, Z.F. Ren, B.Y. Gao, Performance of bimetallic nanoscale zero-valent iron particles for removal of oxytetracycline, J. Environ. Sci., 69 (2018) 173–182.

[13] G.R. Yang, Q.Z. Gao, S.Y. Yang, S.H. Yin, X. Cai, X.Y. Yu, S.S. Zhang, Y.P. Fang, Strong adsorption of tetracycline hydrochloride on magnetic carbon-coated cobalt oxide nanoparticles, Chemosphere, 239 (2020) 124831, doi: 10.1016/j.chemosphere.2019.124831.

[14] Y. Zhang, J.B. Zhou, X. Chen, L. Wang, W.Q. Cai, Coupling of heterogeneous advanced oxidation processes and photocatalysis in efficient degradation of tetracycline hydrochloride by Fe-based MOFs: synergistic effect and degradation pathway, Chem. Eng. J., 369 (2019) 745–757.

[15] T. Saitoh, K. Shibata, K. Fujimori, Y. Ohtani, Rapid removal of tetracycline antibiotics from water by coagulation-flotation of sodium dodecyl sulfate and poly(allylamine hydrochloride) in the presence of Al(III) ions, Sep. Purif. Technol., 187 (2017) 76–83.

[16] F. Deng, L. Zhao, X.B. Luo, S.L. Luo, D.D. Dionysiou, Highly efficient visible-light photocatalytic performance of $Ag/AgIn_5S_8$ for degradation of tetracycline hydrochloride and treatment of real pharmaceutical industry wastewater, Chem. Eng. J., 333 (2018) 423–433.

[17] L.H. Lan, X.W. Kong, H.X. Sun, C.W. Li, D. Liu, High removal efficiency of antibiotic resistance genes in swine wastewater via nanofiltration and reverse osmosis processes, J. Environ. Manage., 231 (2019) 439–445.

[18] W.P. Xiong, G.M. Zeng, Z.H. Yang, Y.Y. Zhou, C. Zhang, M. Cheng, Y. Liu, L. Hu, J. Wan, C.Y. Zhou, R. Xu, X. Li, Adsorption of tetracycline antibiotics from aqueous solutions on nanocomposite multi-walled carbon nanotube functionalized MIL-53(Fe) as new adsorbent, Sci. Total Environ., 627 (2018) 235–244.

[19] N. Neghi, N.R. Krishnan, M. Kumar, Analysis of metronidazole removal and micro-toxicity in photolytic systems: effects of persulfate dosage, anions and reactor operation-mode, J. Environ. Chem. Eng., 6 (2018) 745–761.

[20] D.Y. Wang, H. Luo, L.X. Liu, W. Wei, L.C. Li, Adsorption characteristics and degradation mechanism of metronidazole on the surface of photocatalyst TiO_2: a theoretical study, Appl. Surf. Sci., 478 (2019) 896–905.

[21] M. Ahadi, P. Aberoomand Azar, M.S. Tehrani, S.W. Husain, A comparative study on photodegradation kinetic of tetracycline using visible light sensitized ZnS and Cu-loaded ZnS nanoparticles, J. Appl. Chem., 13 (2018) 249–262.

[22] R.R. Sun, X. Zhang, C.Q. Wang, Y.J. Cao, Co-carbonization of red mud and waste sawdust for functional application as Fenton catalyst: evaluation of catalytic activity and mechanism, J. Environ. Chem. Eng., 9 (2021) 105368, doi: 10.1016/j.jece.2021.105368.

[23] C.Q. Wang, R.R. Sun, R. Huang, Highly dispersed iron-doped biochar derived from sawdust for Fenton-like degradation of toxic dyes, J. Cleaner Prod., 297 (2021) 126681, doi: 10.1016/j.jclepro.2021.126681.

[24] S. Adhami, M. Fazlzadeh, S. Hazrati, Photocatalytic removal of cephalexin by UV/ZnO process from aqueous solutions, J. Environ. Health Eng., 5 (2018) 173–183.

[25] M. Klavarioti, D. Mantzavinos, D. Kassinos, Removal of residual pharmaceuticals from aqueous systems by advanced oxidation processes, Environ. Int., 35 (2009) 402–417.

[26] Y.Y. Gong, J.C. Tang, D.Y. Zhao, Application of iron sulfide particles for groundwater and soil remediation: a review, Water Res., 89 (2016) 309–320.

[27] H. Zhang, L. Peng, A. Chen, C. Shang, M. Lei, K. He, S. Luo, J.H. Shao, Q.R. Zeng, Chitosan-stabilized FeS magnetic composites for chromium removal: characterization, performance, mechanism, and stability, Carbohydr. Polym., 214 (2019) 279–285.

[28] T. Shahryari, A. Mostafavi, D. Afzali, M. Rahmati, Enhancing cadmium removal by low-cost nanocomposite adsorbents from aqueous solutions; a continuous system, Composites, Part B, 173 (2019) 106963, doi: 10.1016/j.compositesb.2019.106963.

[29] N. Nasseh, L. Taghavi, B. Barikbin, M.A. Nasseri, Synthesis and characterizations of a novel $FeNi_3/SiO_2/CuS$ magnetic nanocomposite for photocatalytic degradation of tetracycline in simulated wastewater, J. Cleaner Prod., 179 (2018) 42–54.

[30] D. Ayodhya, G. Veerabhadram, Facile fabrication, characterization and efficient photocatalytic activity of surfactant free ZnS, CdS and CuS nanoparticles, J. Sci.: Adv. Mater. Devices, 4 (2019) 381–391.

[31] Q. Liu, L.-B. Zhong, Q.-B. Zhao, C. Frear, Y.-M. Zheng, Synthesis of Fe_3O_4/polyacrylonitrile composite electrospun nanofiber mat for effective adsorption of tetracycline, ACS Appl. Mater. Interfaces, 7 (2015) 14573–14583.

[32] S.S. Zhang, Y.Y. Sun, F. Liao, Y.W. Shen, H.X. Shi, M.W. Shao, Co_9S_8-CuS-FeS trimetal sulfides for excellent oxygen evolution reaction electrocatalysis, Electrochim. Acta, 283 (2018) 1695–1701.

[33] A. Rahmani-Aliabadi, A. Nezamzadeh-Ejhieh, A visible light FeS/Fe_2S_3/zeolite photocatalyst towards photodegradation of ciprofloxacin, J. Photochem. Photobiol., A., 357 (2018) 1–10.

[34] N. Nasseh, B. Barikbin, L. Taghavi, Photocatalytic degradation of tetracycline hydrochloride by $FeNi_3/SiO_2/CuS$ magnetic nanocomposite under simulated solar irradiation: efficiency, stability, kinetic and pathway study, Environ. Technol. Innovation., 20 (2020) 101035, doi: 10.1016/j.eti.2020.101035.

[35] V. Abdi, Z. Ghasemi, E. Sori nezhad, Biocompatible synthesis of silver-doped titanium dioxide nanoparticles using mangrove, Oceanography, 10 (2019) 123–132.

[36] N. Sreelekha, K. Subramanyam, D. Amaranatha Reddy, G. Murali, K. Rahul Varma, R.P. Vijayalakshmi, Efficient photocatalytic degradation of Rhodamine-B by Fe doped CuS diluted magnetic semiconductor nanoparticles under the simulated sunlight irradiation, Solid State Sci., 62 (2016) 71–81.

[37] Y. Sun, D. Lv, J.S. Zhou, X.X. Zhou, Z. Lou, S.A. Baig, X.H. Xu, Adsorption of mercury(II) from aqueous solutions using FeS and pyrite: a comparative study, Chemosphere, 185 (2017) 452–461.

[38] A.M. Huerta-Flores, L.M. Torres-Martínez, E. Moctezuma, A.P. Singh, B. Wickman, Green synthesis of earth-abundant metal sulfides (FeS_2, CuS, and NiS_2) and their use as visible-light active photocatalysts for H_2 generation and dye removal, J. Mater. Sci.: Mater. Electron., 29 (2018) 11613–11626.

[39] J. William Brown, P.S. Ramesh, D. Geetha, Photodegradation of Methylene blue dye using nanocomposites of copper sulfide doped with Fe/Cd/Zr as nanophotocatalyst, Indian J. Sci. Technol., 12 (2019) 1–11.

[40] Z.Y. Zhang, H.C. Lan, H.J. Liu, J.H. Qu, Removal of tetracycline antibiotics from aqueous solution by amino-Fe(III) functionalized SBA15, Colloids Surf., A, 471 (2015) 133–138.

[41] V.R. Chelli, A.K. Golder, Ag-doping on ZnO support mediated by bio-analytes rich in ascorbic acid for photocatalytic degradation of dipyrone drug, Chemosphere, 208 (2018) 149–158.

[42] R. Benavides, R. González-Hernandez, M.C. González-Cantú, B. Reyes-Vielma, N.C. Billingham, Accelerated degradation of highly loaded polypropylene, J. Vinyl Add. Tech., 9 (2003) 41–49.

[43] J.L. Pablos, C. Abrusci, I. Marín, J. López-Marín, F. Catalina, E. Espí, T. Corrales, Photodegradation of polyethylenes: comparative effect of Fe and Ca-stearates as pro-oxidant additives, Polym. Degrad. Stab., 95 (2010) 2057–2064.

[44] M. Khodadadi, A.H. Panahi, T.J. Al-Musawi, M.H. Ehrampoush, A.H. Mahvi, The catalytic activity of $FeNi_3@SiO_2$ magnetic nanoparticles for the degradation of tetracycline in the heterogeneous Fenton-like treatment method, J. Water Process Eng., 32 (2019) 100943, doi: 10.1016/j.jwpe.2019.100943.

[45] Z.H. Xue, T. Wang, B.D. Chen, T. Malkoske, S.L. Yu, Y.L. Tang, Degradation of tetracycline with $BiFeO_3$ prepared by a simple hydrothermal method, Materials (Basel), 8 (2015) 6360–6378.

[46] Y. Ma, N.Y. Gao, C. Li, Degradation and pathway of tetracycline hydrochloride in aqueous solution by potassium ferrate, Environ. Eng. Sci., 29 (2012) 357–362.

[47] K.-H. Wang, Y.-H. Hsieh, L.-J. Chen, The heterogeneous photocatalytic degradation, intermediates and mineralization for the aqueous solution of cresols and nitrophenols, J. Hazard. Mater., 59 (1998) 251–260.

[48] L.S. Lam, Photocatalytic Degradation of Sunset Yellow Dye Over Zinc Oxide Nanoparticles under Fluorescent Light Irradiation, University Tunku Abdul Rahman, 2016.

[49] Z.Y. Lu, X.X. Zhao, Z. Zhu, Y.S. Yan, W.D. Shi, H.J. Dong, Z.F. Ma, N.L. Gao, Y.S. Wang, H. Huang, Enhanced recyclability, stability, and selectivity of $CdS/C@Fe_3O_4$ nanoreactors for orientation photodegradation of ciprofloxacin, Chem. Eur. J., 21 (2015) 18528–18532.

[50] B.-y. Fan, H.-b. Liu, Z.-h. Wang, Y.-w. Zhao, S. Yang, S.-y. Lyu, A. Xing, J. Zhang, H. Li, X.-y. Liu, Ferroelectric polarization-enhanced photocatalytic performance of heterostructured $BaTiO_3@TiO_2$ via interface engineering, J. Cent. South Univ., 28 (2021) 3778–3789.

[51] H.-w. Wang, X. Fang, Y.-c. Wan, J. Zhan, Z.-j. Wang, H. Liu, Visible-light-induced $NiCo_2O_4@Co_3O_4$ core/shell heterojunction photocatalysts for efficient removal of organic dyes, J. Cent. South Univ., 28 (2021) 3040–3049.

[52] J.B. Wang, D. Zhi, H. Zhou, X.W. He, D. Zhang, Evaluating tetracycline degradation pathway and intermediate toxicity during the electrochemical oxidation over a Ti/Ti$_4$O$_7$ anode, Water Res., 137 (2018) 324–334.

[53] N. Nasseh, A.H. Panahi, M. Esmati, N. Daglioglu, A. Asadi, H. Rajati, F. Khodadoost, Enhanced photocatalytic degradation of tetracycline from aqueous solution by a novel magnetically separable FeNi$_3$/SiO$_2$/ZnO nano-composite under simulated sunlight: efficiency, stability, and kinetic studies, J. Mol. Liq., 301 (2020) 112434, doi: 10.1016/j.molliq.2019.112434.

[54] N. Barhoumi, H. Olvera-Vargas, N. Oturan, D. Huguenot, A. Gadri, S. Ammar, E. Brillas, M.A. Oturan, Kinetics of oxidative degradation/mineralization pathways of the antibiotic tetracycline by the novel heterogeneous electro-Fenton process with solid catalyst chalcopyrite, Appl. Catal., B, 209 (2017) 637–647.

[55] C.Q. Wang, R.R. Sun, R. Huang, H. Wang, Superior Fenton-like degradation of tetracycline by iron loaded graphitic carbon

[56] R. Nosrati, A. Olad, R. Maramifar, Degradation of ampicillin antibiotic in aqueous solution by ZnO/polyaniline nanocomposite as photocatalyst under sunlight irradiation, Environ. Sci. Pollut. Res., 19 (2012) 2291–2299.

[57] G. Safari, M. Hoseini, H. Kamali, R. Moradirad, A.H. Mahvi, Photocatalytic degradation of tetracycline antibiotic from aqueous solutions using UV/TiO$_2$ and UV/H$_2$O$_2$/TiO$_2$, J. Health Hyg., 5 (2014) 203–213.

[58] M. Zhang, W.Q. Song, Q.L. Chen, B.J. Miao, W.C. He, One-pot synthesis of magnetic Ni@Mg(OH)$_2$ core–shell nanocomposites as a recyclable removal agent for heavy metals, ACS Appl. Mater. Interfaces, 7 (2015) 1533–1540.

derived from microplastics: synthesis, catalytic performance, and mechanism, Sep. Purif. Technol., 270 (2021) 118773, doi: 10.1016/j.seppur.2021.118773.

Supplementary information

Table S1
Comparison with previously published reports

Reference	Contaminant	Nanocomposite	Dose	Type of light	Time	%
[S1]	TC	$Ag/AgIn_5S_8$	2.5% $Ag/AgIn_5S_8$	Visible light	Short time	95/8%
[S2]	TC	Ti-doped MCM-41 with different Si/Ti molar ratios	0.1 g/L	Low pressure mercury lamp	150 min	99%
[S3]	TC	Graphene oxide/magnetite/ cerium-doped titania	0.5 g/L	Visible light	60 min	83%
[S4]	TC	$PVDF-TiO_2@g-C_3N_4$	0.2 g/L	Visible light	300 min	90%
[S5]	TC	$FeNi_3/SiO_2/CuS$	0.005 g/L	UV-A	200 min	100%
[S6]	TC	$FeNi_3/SiO_2/ZnO$	0.02 g/L	Simulated sunlight	200 min	100%

S1. References

[S1] F. Deng, L. Zhao, X.B. Luo, S.L. Luo, D.D. Dionysiou, Highly efficient visible-light photocatalytic performance of $Ag/AgIn_5S_8$ for degradation of tetracycline hydrochloride and treatment of real pharmaceutical industry wastewater, Chem. Eng. J., 333 (2018) 423–433.

[S2] K. Zhou, X.-D. Xie, C.-T. Chang, Photocatalytic degradation of tetracycline by Ti-MCM-41 prepared at room temperature and biotoxicity of degradation products, Appl. Surf. Sci., 416 (2017) 248–258.

[S3] M.H. Cao, P.F. Wang, Y.H. Ao, C. Wang, J. Hou, J. Qian, Visible light activated photocatalytic degradation of tetracycline by a magnetically separable composite photocatalyst: graphene oxide/magnetite/cerium-doped titania, J. Colloid Interface Sci., 467 (2016) 129–139.

[S4] X.R. Zheng, Y.Q. Liu, X.B. Liu, Q.B. Li, Y.M. Zheng, A novel $PVDF-TiO_2@g-C_3N_4$ composite electrospun fiber for efficient photocatalytic degradation of tetracycline under visible light irradiation, Ecotoxicol. Environ. Saf., 210 (2021) 111866, doi: 10.1016/j.ecoenv.2020.111866.

[S5] N. Nasseh, L. Taghavi, B. Barikbin, M.A. Nasseri, Synthesis and characterizations of a novel $FeNi_3/SiO_2/CuS$ magnetic nanocomposite for photocatalytic degradation of tetracycline in simulated wastewater, J. Cleaner Prod., 179 (2018) 42–54.

[S6] N. Nasseh, T.J. Al-Musawi, M.R. Miri, S. Rodriguez-Couto, A.H. Panahi, A comprehensive study on the application of $FeNi_3@SiO_2@ZnO$ magnetic nanocomposites as a novel photo-catalyst for degradation of tamoxifen in the presence of simulated sunlight, Environ. Pollut., 261 (2020) 114127, doi: 10.1016/j.envpol.2020.114127.